Impact of Protein Modification on the Protein Corona on Nanoparticles and Nanoparticle–Cell Interactions

Lennart Treuel,[†,‡,§,#] Stefan Brandholt,[†,#] Pauline Maffre,[†,#] Sarah Wiegele,[†] Li Shang,[†] and G. Ulrich Nienhaus[†,⊥,∥,*]

[†]Institute of Applied Physics and Center for Functional Nanostructures (CFN), Karlsruhe Institute of Technology (KIT), 76128 Karlsruhe, Germany, [‡]Institute of Physical Chemistry, University of Duisburg-Essen, 45141 Essen, Germany, [§]Fraunhofer ICT-IMM, 55129 Mainz, Germany, [⊥]Department of Physics, University of Illinois at Urbana-Champaign, Urbana, Illinois 61801, United States, and [∥]Institute of Toxicology and Genetics, Karlsruhe Institute of Technology (KIT), 76344 Eggenstein-Leopoldshafen, Germany. [#]These authors have contributed equally to the manuscript.

ABSTRACT Recent studies have firmly established that cellular uptake of nanoparticles is strongly affected by the presence and the physicochemical properties of a protein adsorption layer around these nanoparticles. Here, we have modified human serum albumin (HSA), a serum protein often used in model studies of protein adsorption onto nanoparticles, to alter its surface charge distribution and investigated the consequences for protein corona formation around small (radius ~5 nm), dihydrolipoic acid-coated quantum dots (DHLA-QDs) by using fluorescence correlation spectroscopy. HSA modified by succinic anhydride (HSAsuc) to generate additional carboxyl groups on the protein surface showed a 3-fold decreased binding affinity toward the nanoparticles. A 1000-fold enhanced affinity was observed for HSA modified by ethylenediamine (HSAam) to increase the number of amino functions on the protein surface. Remarkably, HSAsuc formed a much thicker protein adsorption layer (8.1 nm) than native HSA (3.3 nm), indicating that it binds in a distinctly different orientation on the nanoparticle, whereas the HSAam corona (4.6 nm) is only slightly thicker. Notably, protein binding to DHLA-QDs was found to be entirely reversible, independent of the modification. We have also measured the extent and kinetics of internalization of these nanoparticles without and with adsorbed native and modified HSA by HeLa cells. Pronounced variations were observed, indicating that even small physicochemical changes of the protein corona may affect biological responses.

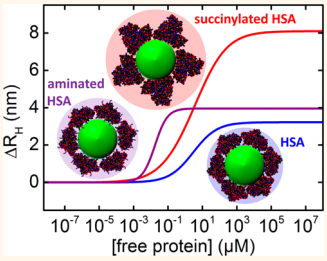

KEYWORDS: quantum dots · nanoparticles · cellular uptake · protein corona · equilibrium constant · binding affinity

Nanoparticles (NPs), which are of similar size as typical biomacromolecular assemblies, are often seen to utilize the endocytosis machinery for intruding cells, where they can give rise to permanent cell damage.[1−3] Wherever NPs encounter biological systems, interactions take place between the NP surfaces and biological components (*e.g.*, proteins, membranes, phospholipids, DNA *etc.*). It has now been well established that proteins from body fluids bind to NP surfaces upon their exposure to an organism,[4−8] forming a so-called "protein corona" around the NPs.[6−10] Consequently, living systems usually interact with protein-coated rather than bare NPs,[6,10] and the structure, dynamics and stability of the corona can be decisive factors governing the biological response of an organism to NP exposure.[11] The notions "hard" and "soft" protein corona have been introduced to refer to strongly and weakly bound protein adsorption layers on the NP surface.[6] It is evident that, upon exposure of NPs to a mixture of proteins with different binding properties such as blood serum, the fastest binders will form the initial corona. They will, however, subsequently be replaced by proteins with the highest affinity to the surface (Vroman effect). Thus, one may initially observe a "soft" corona forming on short time scales (seconds to minutes) that subsequently evolves into a "hard" corona over periods of hours.[12]

In recent years, a wide variety of different NPs have been synthesized, with different surface chemical properties, ranging from bare inorganic surfaces over organic coatings to intricate polymeric structures. Proteins may interact with these surfaces in different ways, depending on the detailed surface chemistry. Proteins are flexible biomolecules that are known to fluctuate among a vast number of different conformations at

* Address correspondence to uli@uiuc.edu.

Received for review September 26, 2013 and accepted December 30, 2013.

Published online December 30, 2013
10.1021/nn405019v

room temperature.[13] Because proteins are on the brink of stability, they may experience interactions with some types of surfaces that are strong enough to cause denaturation or significantly change their conformations,[14−16] with concomitant loss of their biological function.[17,18] Structural changes in the protein may cause exposure of new antigenic sites, "cryptic" peptide epitopes,[10,19] potentially triggering an immune response,[20,21] which, if launched against a self-protein, can promote autoimmune diseases.[22]

Mechanistic details of protein structural changes at NP surfaces have still remained elusive.[22−25] Understanding the formation and persistence of the protein corona is a critical issue, however, not only for the elucidation, interpretation and assessment of biological effects of unintended exposure to NPs, but also for their intended use in nanomedicine. Numerous efforts have been made to design specific NP surfaces enabling targeted transport of drugs or vaccines,[23,26−31] but more based on intuition rather than detailed mechanistic knowledge.[1] Whereas many studies have focused on varying NP properties such as hydrophobicity, zeta potential, drug release properties and biological behavior,[23,30,32−46] it appears that controlling the protein corona formation is a prerequisite of any strategy aimed at targeted drug delivery.

Our group has introduced fluorescence correlation spectroscopy (FCS) as a highly precise method to simultaneously determine binding affinities of proteins to nanoparticles and the thickness of the protein corona.[8,47] This method permits the quantitative observation of protein adsorption *in situ*, whereas most other methods require a separation of NPs and protein-containing solution after incubation and prior to the analysis. *In vitro* studies of important human blood serum proteins (HSA, transferrin, apolipoprotein A-I and apolipoprotein E4) adsorbing onto negatively charged FePt NPs carrying carboxyl groups revealed that the thickness of the protein corona is a well-defined quantity, correlated with the molecular dimensions of the protein molecules.[8,47] The corona always consisted of a monolayer of protein molecules binding in a certain orientation to the NP surface, and the observed specific orientations of the corona proteins were such that they permit optimal electrostatic interactions between positively charged patches on the proteins and the negatively charged surfaces of the NPs.[47] Importantly, local charge distributions in the binding interfaces mediate the interaction rather than the net charge of the proteins and NPs because, at typical ionic strengths of biological media (∼150 mM), Debye screening is efficient, so charge interactions are only short-ranged (∼1 nm).

The intriguing revelation of a close structure-affinity relation[47] opens a promising new perspective for chemical approaches to change the protein corona characteristics by altering the charge distribution on the protein surface. Here, we have modified the surface charge characteristics of human serum albumin (HSA) by succinylation or amination and studied the effect of these modifications on the formation of a protein corona around CdSe−ZnS core−shell quantum dots (QDs) (radius ∼5 nm) functionalized with dihydrolipoic acid (DHLA). We have also probed the extent and kinetics of cellular uptake of QDs enshrouded by native and modified HSA and compared these data to the uptake of bare QDs. These data show that even small physicochemical changes in the corona proteins may elicit different biological responses.

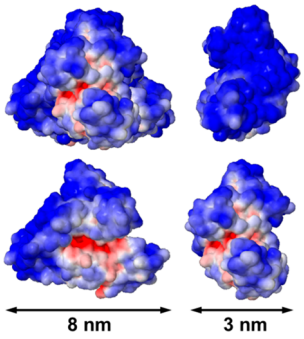

Figure 1. Space-filling models of human serum albumin (PDB code: 1UOR) colored to indicate the surface electrostatics at pH 7.4 (blue, negative potential; red, positive potential; range from $-5\ k_BT/e$ to $+5\ k_BT/e$; calculated online at http://nbcr-222.ucsd.edu/pdb2pqr/[49]).

RESULTS AND DISCUSSION

Charge Modification of HSA. The shape of the folded polypeptide chain of HSA can be well approximated by an equilateral triangular prism, with triangle sides of 8.4 nm and a height of 3.15 nm.[48] Our earlier FCS studies of the association of HSA to negatively charged, carboxylic acid functionalized NPs[47] revealed a thickness of the protein corona of ∼3.3 nm, which is compatible with binding of the HSA molecules to the NPs *via* their triangular sides. The electric surface potential of native HSA[49] shows distinct, positively charged patches (Figure 1) that mediate the Coulombic interaction.

These positive patches arise from the presence of the basic lysine and arginine amino acid residues (Supporting Information, Figure S1), which each carry a positive charge on their side chains in a solvent-accessible environment at physiological, *i.e.*, near-neutral pH. Succinic anhydride reacts with the ε-amino group of lysine, turning it into a negatively charged carboxylate function.[50−53] We used this reaction at pH 7.4 to modify a fraction of lysine residues on the protein surface to obtain succinylated HSA (HSAsuc). The negative patches of HSA arise from aspartic and glutamic acid residues, which each carry a carboxyl function and, thus, a negative charge at physiological pH. In the presence of 1-ethyl-3-(3-dimethylamino-propyl)-carbodiimide (EDC) as a catalyst, a fraction of the

carboxyl groups was reacted with ethylenediamine to convert them into positively charged amino groups to obtain aminated HSA (HSAam).

As expected, succinylation significantly lowered the negative zeta potential from (−10.5 ± 1.3) mV for native HSA to (−19 ± 4) mV for HSAsuc, whereas amination increased it to (−6.1 ± 0.4) mV, in phosphate buffered saline (PBS), pH 7.4. The hydrodynamic radius was measured by dynamic light scattering (DLS), yielding (3.20 ± 0.04) nm for native HSA, (3.3 ± 0.2) nm for HSAsuc, and (3.1 ± 0.1) nm for HSAam. Thus, the size remained essentially unchanged within the measurement error, so we can firmly conclude from these data that the overall protein fold is still maintained after chemical modification.

Quantitative Analysis of Protein Corona Formation on DHLA-QDs. To investigate the effect of the altered protein charge characteristics on protein corona formation, we have measured the interactions of HSA, HSAsuc and HSAam with negatively charged, carboxyl-functionalized CdSe−ZnS core−shell QDs, which were water-solubilized with a DHLA ligand shell. Their zeta potential in PBS was (−31.2 ± 0.8) mV.

To quantitatively monitor HSA adsorption onto DHLA-QDs, we used fluorescence correlation spectroscopy (FCS), a technique that is based on the analysis of fluorescence bursts emitted by particles diffusing through a tiny observation volume (*ca.* 10^{-15} L) formed by tight focusing of a laser beam.[8,54−56] Autocorrelation analysis of the fluorescence emission time traces yields a characteristic time scale of diffusion, τ_D, from which the diffusion coefficient, D, and, by means of the Stokes−Einstein relation, the hydrodynamic radius r_h can be extracted. This approach permits the direct, *in situ* observation of the QD size increase as a consequence of protein binding to its surface.[8,47] The resulting data can be quantitatively analyzed by a simple model, where the shape of the QD with bound proteins is approximated by a sphere. Then, r_h changes with the number of proteins, N, bound to the NP surface according to

$$r_h(N) = \sqrt[3]{\frac{3}{4\pi}(V_0 + N \cdot V_P)} \quad (1)$$

Here, V_0 is the volume of the bare QD, N is the number and V_P is the molecular volume of the adsorbed proteins. Note that this ansatz assumes a dense coating only by protein molecules. We may, however, envision that some water molecules may also become arrested on the NP along with the proteins, which would then contribute in proportion to the proteins. In this case, V_P should be replaced by an effective volume that takes the hydration water into account. Since the typical protein density equals 1.35 g mL^{-1}, the protein volume is in a good approximation proportional to the mass. Introducing the radius of the bare QD, $r_h(0)$, which is (4.8 ± 0.2) and (5.6 ± 0.1) nm for the QD preparations used in this work, and the coefficient $c = V_P/V_0$, we obtain

$$r_h(N) = r_h(0)\sqrt[3]{1 + c \cdot N} \quad (2)$$

In FCS measurements of protein adsorption onto nanoparticles with a variety of serum proteins, we have always observed saturation of the radius increase at high protein concentrations, indicating formation of a protein monolayer. Therefore, there is a finite number of binding sites available on the NP, and the dependence of N on the concentration of free protein in the solution, [P], can be modeled in the simplest fashion by the Hill equation,[8]

$$N = N_{max}\frac{1}{1 + (K'_D/[P])^n} \quad (3)$$

where the number of binding sites, *i.e.*, the maximum number of proteins binding to the NPs is represented by N_{max}, and K'_D denotes the midpoint of the transition, *i.e.*, the concentration of protein molecules free in solution when 50% of the binding sites are filled. This parameter thus quantifies the strength of the NP−protein interaction. The Hill coefficient, n, controls the steepness of the curve and contains information about the cooperativity of binding.

FCS autocorrelation curves were measured to determine the affinities of HSA, HSAsuc and HSAam toward DHLA QDs, using protein concentrations ranging from 0.2 nM to 1.05 mM. The autocorrelation functions at each concentration were fitted with a model function to extract the correlation time τ_D. The diffusion coefficients were then calculated based on the known extension of the focal spot so that, finally, radii of hydration were determined as a function of concentration.[8] For native HSA (Figure 2a), we found an overall increase of the hydrodynamic radius from $r_h(0)$ = (4.8 ± 0.2) nm for bare QDs to $r_h(N_{max})$ = (8.1 ± 0.4) nm at a protein concentration of 200 μM, where there is saturation, indicating that the QDs are fully covered by a protein monolayer. The radius increase, Δr_h = (3.3 ± 0.6) nm, is compatible with complete surface coverage by HSA molecules adsorbing with their triangular faces to the QD (Figures 1 and 2b), as was shown earlier for different types of negatively charged, carboxyl-functionalized NPs of similar size.[8] Quantitative analysis of these data with the Hill equation revealed a maximum number of surface bound proteins of $N_{max} = 18 \pm 2$ and a $K'_D = (6.4 \pm 3.6)$ μM. The Hill coefficient of n = 0.7 ± 0.2 indicates an anticooperative binding behavior, which is also in line with previous experiments investigating HSA adsorption onto polymer-coated FePt NPs[8,47] and QDs.[8] These results indicate that HSA molecules bind in such orientations on the NP surfaces, for which there are optimal attractive interactions between the positively charged patches on the proteins and the negatively charged QD surfaces, supporting the interpretation by Maffre *et al.*[47]

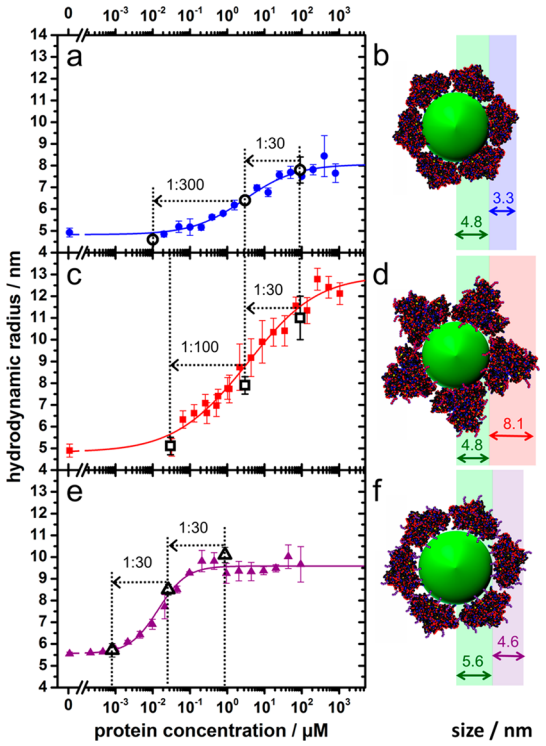

Figure 2. Adsorption of (a and b) HSA, (c and d) HSAsuc and (e and f) HSAam onto DHLA-QDs. Filled symbols: Hydrodynamic radii of DHLA-QDs plotted as a function of the concentration of (a) HSA, (c) HSAsuc and (e) HSAam free in solution. Solid lines represent fits of eqs 2 and 3 to the data. Open symbols: Hydrodynamic radii measured at 90 μM (a) HSA and (b) HSAsuc and 0.9 μM (e) HSAam and after two successive dilution steps as shown in the graphs. (b, d, and f) Schematic depictions of the hydrodynamic radii increasing as a result of protein adsorption, with (b) native HSA and (f) HSAam shown adsorbing with their triangular faces, leading to a radius increase of 3.3 and 4.6 nm, respectively, and (d) HSAsuc adsorbing with the edge of the prism, causing a radius increase of 8.1 nm.

The protein adsorption data using charge-modified HSAsuc (Figure 2c) show a distinctly different behavior, with the QD radius increasing from $r_h(0)$ = (4.8 ± 0.2) nm for bare QDs to $r_h(N_{max})$ = (12.9 ± 0.4) nm for QDs with a fully formed corona. Therefore, the thickness increase, Δr_h = (8.1 ± 0.6) nm, is much greater than for native HSA, which can be explained by binding of HSAsuc molecules to the QD surface in such an orientation that the triangular sides are perpendicular to the surface. Such an orientation yields 7.3 nm for binding with one of the rectangular faces and 8.4 nm for a perpendicular arrangement of one of the sides of the triangle (Figures 1 and 2d). We note that HSAsuc is also slightly larger than the native form due to the succinylated lysine side chains. Quantitative evaluation using the Hill equation revealed a maximum number of surface bound HSAsuc molecules of N_{max} = 89 ± 8, K'_D = (19 ± 8) μM, and n = 0.52 ± 0.04 suggests an enhanced anticooperativity. We note that the N_{max} parameter appears inflated because the analysis rests on the assumption that the additional volume occupied by HSAsuc molecules is densely filled. A side-on orientation, as depicted in Figure 2b, may not accommodate such an arrangement. The estimation assuming that the HSAsuc molecules bind with their rectangular sides yields a lower bound of ~11 molecules, which appears too small because HSA molecules can also bind with their triangular tips. In this case, they have a much smaller footprint. Because the precise protein:NP stoichiometry is not relevant for this work, we have not dwelled on this issue further.

For HSAam, the QD radius was observed to increase from $r_h(0)$ = (5.6 ± 0.1) nm for the bare QDs to $r_h(N_{max})$ = (10.2 ± 0.1) nm for the fully loaded NP. The change in radius, Δr_h = (4.6 ± 0.1) nm, is larger than for native HSA. This difference appears quite reasonable because native HSA adsorbs in a specific orientation, *i.e.*, *via* one of the triangular faces. Modification of the protein with additional amine functions is expected to randomly enhance already present positive patches or generate entirely new ones. Protein adsorption *via* other positive patches sites may lead to a variety of HSAam orientations and thus an increased corona thickness. Interestingly, the midpoint concentration, K'_D = (22 ± 3) nM, indicates that the amino modification gives rise to an enormous, ~1000-fold increase in binding affinity. This finding supports our view that the affinity is largely governed by electrostatic interactions. The interactions between DHLA-QDs and HSAam are apparently much stronger because of a higher density of positively charged groups on the protein surface. The Hill coefficient, n = 1.2 ± 0.1, is greater than for native HSA (enhanced cooperativity), and the maximum number of proteins bound is N_{max} = 31 ± 1. (Note that we did not account for a possible slight volume increase of the protein due to its chemical modification, which would lower N_{max}.)

The observed differences in the coronae formed by adsorption of native HSA, HSAsuc and HSAam are intriguing. The absolute change of NP size by ~8 nm upon HSAsuc adsorption is compatible with binding in a distinctly different orientation than native HSA, with the ~8 nm side of the trilateral prism extending radially rather than the 3.15 nm side (Figure 2d). Presumably, succinylation reduces the stabilizing Coulombic interaction *via* the positive patch on the triangular face to such an extent that other epitopes located on the edges of the prism provide stronger binding. In fact, the decreased binding affinity by a factor of 3 for HSAsuc indicates an overall weakening of the interaction by ~3 kJ/mol. In contrast, the radius increase by Δr_h = (4.6 ± 0.1) nm with HSAam suggests that the aminated proteins adsorb differently from native HSA, likely in heterogeneous orientations because of different positions of the positive patches generated by chemical modification. The affinity of HSAam toward the negatively charged QDs was increased by a factor of ~1000, which corresponds to a strengthening of the

interaction by ~17 kJ/mol. This stabilization is striking, considering that the net charge of the protein is still negative. Nevertheless, the increased density of the positively charged groups on the protein surface apparently gave rise to a drastic increase the binding affinity. We have also observed very strong protein adsorption when using HSAam preparations with a higher degree of amination and thus an overall positive zeta potential of the protein-bound DHLA-QDs (data not shown). However, we were unable to measure complete binding isotherms due to lacking colloidal stability at intermediate degrees of NP loading with proteins, for which the overall zeta potential was close to zero.

We stress that an explanation of the variation in corona thickness as a consequence of denaturation of our modified proteins appears unrealistic because the DLS measurements confirmed that HSAsuc and HSAam are compact and properly folded, as expected from the rather mild succinylation and amination procedures. Moreover, the experiments on the reversibility of protein corona formation discussed below further strengthen our claim that HSAsuc and HSAam retain their overall native fold in solution and upon adsorption onto the NPs.

Reversibility of Protein Adsorption. In many studies aimed at the characterization of the protein corona, NPs are exposed to biological liquids and, subsequently, the NPs are separated from those liquids by harsh and lengthy treatments such as centrifugation, chromatography and repeated washing steps to study their adsorption layer. Such analyses can only reveal those proteins that are tightly, preferentially covalently, bound to the NPs, *e.g.*, proteins bound to gold NPs *via* multiple thiol groups from cysteine residues. Usually, proteins have to unfold and form a "hard" corona to establish these strong, persistent interactions. However, many engineered NPs are enshrouded by tailor-made, often polymeric surfaces that only weakly interact with proteins. In biological fluids, these NPs will also be coated with proteins,[47,57] but such a "soft" corona would quickly decompose when attempting to separate the NPs from the liquids. Therefore, such a soft corona can only be measured *in situ*, while the NPs are exposed to the biofluid, as we have done here by using the FCS method.

Still, a key question is if binding isotherms as those in Figure 2 reflect true equilibrium, *i.e.*, are the kinetics of protein adsorption and desorption sufficiently fast so that equilibrium is established prior to the measurement? To test reversibility of protein binding and, hence, the validity of an equilibrium treatment, we prepared QDs in a PBS solution containing free HSA at a concentration of 90 μM to ensure that the corona was essentially fully formed (Figure 2a). We then diluted the solution down to 3 μM (1:30) and, in a second step (1:300), down to 10 nM HSA. Hydrodynamic radii of the suspensions were measured by using FCS after 90 min of equilibration, yielding $r_h = (7.8 \pm 0.6)$, (6.4 ± 0.2) and (4.6 ± 0.2) nm for 30 μM, 3 μM and 10 nM HSA free in solution, respectively. All three points of this controlled desorption experiment lie on the HSA binding curve within the experimental error (Figure 2a). The same procedure was applied to a solution of QDs carrying a HSAsuc corona, with dilution steps from 90 to 3 μM (1:30) and further to 30 nM (1:100), yielding $r_h = (11.2 \pm 0.2)$, (7.6 ± 0.1) and (5.2 ± 0.3) nm, respectively, for the three HSAsuc concentrations. Likewise, for HSAam at 0.9 μM, 30 nM and 1 nM, we obtained $r_h = (10.1 \pm 0.4)$, (8.5 ± 0.2), and (5.7 ± 0.3) nm, respectively. Again, these points lie on the original binding curve within the error (Figure 2c,e).

The reversibility of the NP size change observed here is strong evidence that we measure protein adsorption in true equilibrium and is a most interesting case study in the ongoing discussion within the field regarding the validity of equilibrium approaches to describe protein adsorption onto NP surfaces.[57] The thin solubilization layer surrounding the inorganic core–shell structure of DHLA-QDs may support reversibility of protein binding. Other NP systems, however, may be markedly different in this respect. For example, on NPs with long-chain polymer coatings, entanglement of polymer chains and protein moieties may induce protein denaturation and hamper protein desorption.

Influence of Protein Adsorption on Cellular Uptake. To investigate the biological implications of the changed protein corona due to charge modification, we studied internalization of DHLA-QDs with native and modified HSA coronae by HeLa cells and compared the results to the uptake behavior of DHLA-QDs without a protein corona. Representative cell images are shown in Figure 3a–d. Upon QD internalization, clusters of QDs were observed in the perinuclear region of the cell. Earlier, quantitative studies of cellular uptake with D-penicillamine coated QDs (DPA-QDs) of similar size (~10 nm diameter) as the DHLA-QDs used here,[58] and also with much larger polymeric nanoparticles (~100 nm diameter),[59,60] revealed that the NPs are predominantly internalized by the cells *via* active, pinocytic (mainly clathrin-mediated) pathways and end up in endosomes and lysosomes. Passive transport may also occur, but with a much lower yield so that it remains unnoticed as long as active transport is present.[61]

We quantified the fluorescence intensities of the membrane associated and intracellular fractions of QDs (Figure 3e). Incubation with bare QDs resulted in the largest amount of QDs on the membrane and in the cells. Binding to the plasma membrane is a crucial first step mediated by cell surface receptors that recognize the NP surface and activate the endocytosis machinery. For small NPs (~10 nm diameter), we typically observe them coating the plasma membrane upon exposure,[62]

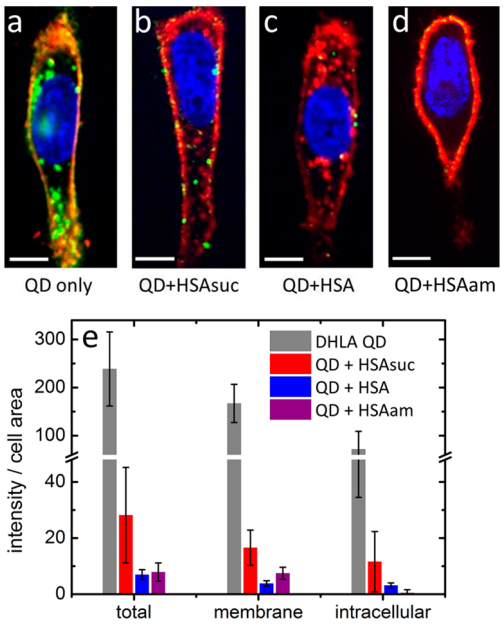

Figure 3. Uptake of DHLA-QDs by HeLa cells. Cells were incubated for 2 h with 10 nM QDs in PBS (a) without protein, (b) with 100 μM HSAsuc, (c) with 100 μM native HSA and (d) with 100 μM HSAam. The cell membrane is shown stained in red, nucleus in blue, and QDs in green. Scale bar, 10 μm. (e) Quantification of NP uptake after 2 h using *ca.* 10 cells from two independent measurements. Error bars represent standard deviations due to cell-to-cell variations.

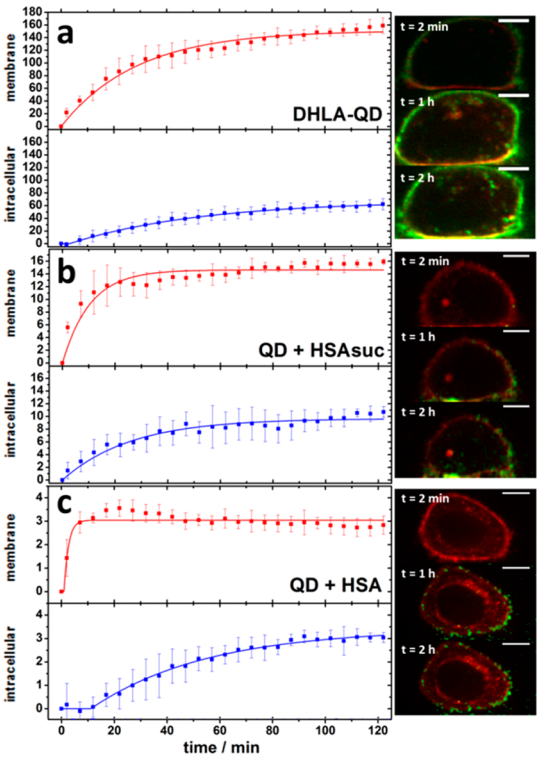

Figure 4. Kinetics of DHLA-QD uptake by HeLa cells from quantitative analysis of spinning disk confocal fluorescence images (examplary cells are shown on the right; red, membrane stain; green, QDs; yellow, colocalization, scale bar, 10 μm). Time evolution of the membrane associated and internalized fractions are shown for incubation with (a) DHLA-QDs in PBS only, (b) DHLA-QDs in PBS plus 100 μM HSAsuc and (c) DHLA-QDs in PBS plus 100 μM native HSA. Error bars represent standard deviations from the mean.

whereas larger NPs (~100 nm) were not noticeably present at the membrane but, nevertheless, appeared inside the cell.[60] Therefore, it has been suggested that a small NP may not be able to trigger endocytosis by itself because it interacts with an insufficient number of receptors. Instead, a critical local density of QDs on the cell membrane is required to initiate the active internalization process.[57,58]

From the data in Figure 3e, it is evident that the presence of a protein corona markedly suppresses membrane binding and uptake of DHLA-QDs by the cells, as was observed earlier for other adsorbed proteins and polymer-coated NPs.[62−67] Compared with native HSA, uptake suppression is less pronounced for NPs coated with HSAsuc. In view of the decreased affinity of HSAsuc toward DHLA-QDs, such an effect would be expected if shedding of the adsorption layer were to happen prior to NP binding to the cell membrane, *e.g.*, to scavenger receptors.[68,69] For DHLA-QDs with bound HSAam, we have observed slightly enhanced binding to the cell membrane compared to native HSA, which may be due to the less repulsive electrostatic interactions between the NPs and the negatively charged cell surface. Notably, internalization of HSAam-coated NPs by the cells was suppressed to a level below the detection threshold. One could speculate that, if corona shedding is required to activate endocytosis, the tight binding of HSAam to the NP surface can prevent this process. However, in general, the distinctly different structures of the protein coronae reported here, which expose different epitopes to the cell receptors, will give rise to the different extent of uptake. Studies to monitor the fate of the protein corona during internalization and within the cell are currently ongoing in our laboratory.

NP Uptake Kinetics. We further investigated the time dependence of NP uptake by HeLa cells for 2 h by using spinning disk confocal microscopy. Confocal images were acquired every 5 min for up to ten cells in a single field of view, and at least two independent measurements were carried out for incubation of cells with NPs in PBS and PBS supplemented with 100 μM HSA or HSAsuc. Kinetics of HSAam-coated NPs are not presented because of their negligible internalization (Figure 3d,e). In the image analysis, we again separated the data into membrane associated and intracellular fractions.[58] In Figure 4 a−c, the time-dependent averaged intensities of the two fractions are plotted as a function of time for all four particle types. Close-up views of individual cells after 2, 60, and 120 min of NP incubation are also shown as examples to the right of the kinetics. The kinetics of NP uptake, $N(t)$, can be fitted with an exponential function, which we adapted from a previously described model,[69] by adding a time

TABLE 1. Fit parameters of Cellular Uptake Kinetics

	membrane associated			intracellular		
	τ_m (min)	t_0 (min)	$N_{m,sat}$, (au)	τ_i (min)	t_0 (min)	$N_{i,sat}$ (au)
DHLA-QD	29 ± 2	≤1	151 ± 3	50 ± 3	3.2 ± 0.8	68 ± 1
QD + HSAsuc	10 ± 2	<2	14.6 ± 0.3	26 ± 3	<2	9.6 ± 0.3
QD + HSA	1.7 ± 0.8	<1	3.04 ± 0.05	44 ± 4	11 ± 1	3.4 ± 0.1

delay, t_0, which has also been observed in similar data before.[70]

$$N(t) = N_{sat}(1 - \exp(-(t - t_0)/\tau)) \text{ for } t \geq t_0,$$
$$N(t) = 0 \text{ for } t < t_0 \quad (4)$$

Here, N_{sat} is the number of NPs at saturation and τ is the lifetime parameter of the exponential. In our experiments, N_{sat} cannot be quantified in terms of the real number of NPs and serves as an amplitude scaling factor here. The parameters obtained from the fits of the data with eq 4 are compiled in Table 1.

All QDs started to accumulate at the plasma membrane of HeLa cells within minutes after exposure. The quantitative analysis of this behavior revealed that the characteristic times for QD association to the membrane, τ_m, varied from <2 (HSA) over 10 (HSAsuc) to ~30 min (bare QDs). The marked acceleration by a factor of ~15 from bare to HSA-coated NP uptake goes hand in hand with a drastic decrease in the membrane deposition level in equilibrium by a factor of ~50. Within a simple two-state kinetic model governed by an on- and an off-rate coefficient, these two observations taken together indicate that the off-rate coefficient is much larger for HSA-coated NPs, which indicates weaker binding to the membrane. As a consequence, we observed faster kinetics with concomitant saturation at a smaller amplitude. The data for HSAsuc-coated NPs are in-between bare and HSA-coated NPs, which would imply a tighter binding to the membrane than for HSA, either mediated by the modified protein itself or its dissociation prior to NP adsorption to the plasma membrane.

Unlike the characteristic times for membrane association, τ_m, the rate coefficients for internalization, τ_i, vary only within less than a factor of 2 (Table 1), suggesting that this parameter is largely controlled by the cellular endocytosis machinery. Even for NPs enshrouded by HSA, where membrane association is in steady state within a few minutes, the subsequent internalization occurs on the hour time scale. These well-separated time scales imply that the overall uptake yield is controlled by the availability of NPs on the plasma membrane and thus by the varying membrane affinities of the different QD types.

It is interesting that a clearly noticeable lag time in the uptake is only observed for the HSA-coated QDs, which showed the smallest membrane association. Intriguingly, this behavior again fits well to the previous studies of Jiang *et al.*,[58] who argued for the necessity of a critical threshold density of QDs on the cell membrane to trigger active internalization. The low equilibrium membrane binding of the HSA-coated QDs should lead to a longer delay time until a threshold density is exceeded. For the kinetic traces of bare QDs and HSAsuc-coated QDs, the lag time is expected to be shorter. For bare QDs, the fit still yields a lag time, but it is barely above the noise level, and for HSAsuc-coated QDs, none is noticeable, presumably due to the limited accuracy of our data.

CONCLUSIONS

In this study, we found that simple chemical modifications of the surface charge distribution of HSA significantly change the nature of protein adsorption onto DHLA-QDs. These results emphasize the important role of Coulomb interactions in shaping the protein corona.[47] A dependence of the overall protein charge on the adsorption behavior had been proposed earlier,[71−73] but a recent comprehensive study of full serum protein adsorption to negatively charged silica nanoparticles did not find enhanced binding of proteins that were overall positively charged at pH 7.3.[74] This conundrum may, at least partially, be resolved by considering the Debye length at the typical ionic strengths of biological fluids and PBS buffer, which is <1 nm and thus smaller than the size of a protein (a few nanometers). Therefore, Coulomb interactions are essentially only effective between charges located on the NP and protein surfaces that are in close contact.

The modified charge distributions of HSAsuc and HSAam gave rise to significant changes of the binding affinity as well as the orientation in which the proteins adsorb onto the NP. These observations underscore the importance of localized charge clusters governing protein binding onto NP surfaces. Detailed analysis of the electrostatics at the NP-protein interface by computational methods can contribute significantly toward a better understanding of the structure and composition of the protein corona that forms under physiological conditions.[75]

Protein adsorption to DHLA-QDs was observed to be completely reversible and thus can be modeled by using an equilibrium approach. This issue has been debated before,[8,47,57] and we emphasize that it is not a forgone conclusion universally true for every nanoparticle−protein system. With some NP surfaces, protein adsorption leads to tight binding accompanied by a substantial loss of protein structure.[9,76,77] Desorption may be impossible or lead to a denatured protein with modified properties. In any case, the elucidation of general mechanistic details governing the reversibility of protein adsorption onto NP (and other) surfaces remains a challenging issue.

We have further shown that NP uptake by HeLa cells was affected by the details of the protein corona. Our live cell imaging data suggest that the uptake yield

depends on the affinity of the NP toward the plasma membrane. An important issue that has remained elusive, though, is if the proteins dissociate from the NP prior to docking. The enhanced membrane binding of HSAsuc may argue for protein shedding, but another possibility would also be the changed interactions between the modified corona and membrane proteins. Whereas the kinetics of membrane binding depended strongly on the presence and nature of the protein corona, the kinetics of the endocytosis process, once triggered, was not affected by the protein corona. QDs coated with HSAam showed slightly more binding to the plasma membrane than HSA, possibly due to enhanced electrostatic interactions, but the level of internalization was very low.

While this study gives a vivid example of rather small protein modifications affecting their adsorption onto NPs and interactions between NPs and cells, there is still a long way ahead of us to reach a detailed mechanistic understanding of protein corona-mediated nanoparticle interactions with the plasma membrane and the overall NP uptake process.

MATERIALS AND METHODS

QD Synthesis and Characterization. CdSe/ZnS core/shell QDs were synthesized in chloroform as previously reported.[78] Water-soluble, negatively charged nanoparticles were obtained *via* ligand exchange with DHLA.[79] Fluorescence excitation and emission spectra of the DHLA-QDs (Supporting Information, Figure S2) were measured on a Fluorolog-3 FL3-22 (HORIBA Jobin Yvon, Edison, NJ); the emission band had a peak at 605 nm. For relative scaling of fluorescence images, the fluorescence emission from DHLA-QDs in PBS, in PBS with 100 μM HSA, in PBS with 100 μM HSAsuc, and in PBS with 100 μM HSAam was measured as shown in Supporting Information (Figure S3).

Preparation of Modified HSA. Succinylation of serum albumin (purity: ≥98%, SigmaAldrich, Milwaukee, WI) was carried out basically as described by Aitken and Learmonth,[53] with slight modifications. Succinic acid anhydride (purity: ≥99%, SigmaAldrich), dissolved at a concentration of 0.8 M in 1,4-dioxane (p.a., Merck, Darmstadt, Germany), was added in small portions to 100 μL of a 250 μM HSA solution in PBS buffer over a period of 15 min, so that a 50-fold molar excess of succinic acid anhydride was reached. Amination of HSA was performed according to a published procedure (with slight modifications).[80] Briefly, 1 mg of 1-ethyl-3-(3-dimethylaminopropyl)-carbodiimide (EDC, SigmaAldrich) was added to a mixture of 1 mL HSA (10 mg/mL) and 1 mL of ethylenediamine (1 M, Thermo Scientific, Rockford, IL) in PBS. The reaction solution was stirred for 2 h at room temperature. Modified proteins (HSAsuc and HSAam) were purified on a G25 gel column (GE-Healthcare, Munich, Germany).

Dynamic Light Scattering and Zeta Potential Measurements. The experiments were performed on a Zetasizer Nano ZS (Malvern, Herrenberg, Germany). To analyze the results from multiple DLS (zeta potential) measurements, the number (zeta potential) distributions were individually fitted with Gaussian functions to determine the hydrodynamic diameters (zeta potentials). In this work, we present averages of these parameters together with standard deviations from the mean.

FCS Experiments. FCS measurements were performed on a homemade confocal microscope based on an Axiovert 135 TV frame (Zeiss, Göttingen, Germany),[81,82] with slight modifications as follows: 532-nm excitation light (5 to 6 μW power at the focal plane) from a diode-pumped solid state laser (Excelsior 532-100-SLM-CDRH, Newport, Spectra-Physics Laser Division, Irvine, CA) was coupled into the microscope by a single mode fiber and focused into the sample using a water immersion objective (UPLAPO 60×/1.2w, Olympus, Hamburg, Germany). The fluorescence light was collected by the same objective, passed through a homemade acousto-optic beam splitter (AOBS) and focused into a 50 μm-diameter confocal pinhole. After passing through a 532 nm notch filter and a 50/50 beam splitter cube, the light was detected in two separate channels by using avalanche photodiodes (SPCM-AQR 14, Perkin-Elmer, Waltham, MA). The events in the two channels were cross-correlated by a hardware correlator (model 5000/E, ALV, Langen, Germany) to yield the diffusional autocorrelation function. Alternatively, FCS measurements were also performed on a time-resolved confocal microscope (Microtime 200, PicoQuant, Berlin, Germany). The QDs were excited by a continuous-wave 485-nm diode laser (LDH-D-C-485, Picoquant, Berlin, Germany) focused by an objective (UPLSAPO 60XW, Olympus, Hamburg, Germany). Fluorescent light was collected by the same objective, passed through the dichroic mirror and a 585/65 nm filter, before being focused into a 75 μm pinhole. The light was then collimated, split by a 50/50 beam splitter cube and focused onto two avalanche photodiode detectors (SPCM-AQR-13, Perkin-Elmer, Rodgau, Germany). Cross-correlation of the fluorescence time traces recorded by the two detectors was subsequently performed by commercial software (Sympho Time, Picoquant). All measurements were performed at 23 °C. Particle solutions were diluted to ~2 nM with PBS; HSA was diluted to the desired concentrations with PBS and mixed in equal volumes with the diluted particle solutions. The samples were incubated for 10 min prior to the measurements. Rhodamine 6G or Atto488 was used as a reference sample (diffusion coefficients $D = (4.14 \pm 0.05) \times 10^{-6}$ cm^2 s^{-1} and $D = (4.0 \pm 0.1) \times 10^{-6}$ cm^2 s^{-1} at 25 °C, respectively) for calibrating the detection volume.[83]

Due to the high affinity of HSAam toward the QDs, it was necessary to work with very small protein concentrations, and, thus, the proteins were not in excess in solution compared to the QDs. Consequently, the concentration of free protein in solution had to be calculated from the known total concentration of protein mixed with the QDs. This was achieved by using the concentration of QDs measured by FCS and by estimating the number of proteins bound based on the measured size of the QDs. The number of proteins bound was estimated by the volume model described in this paper (maximal estimation), as well as by a surface model (minimal estimation) and the average was taken for further analysis of the data.

Measurement of Protein Binding Isotherms. HSA and HSAsuc stock solutions (1.8 mM) were prepared by mixing lyophilized HSA with PBS buffer or, for HSAsuc, by increasing the protein concentration after succinylation and purification using a centrifugation size exclusion filter (Vivaspin 500, cutoff 5 kDa, Sartorius, Göttingen, Germany). For HSAam, the stock solution (186 μM) was used as obtained from its preparation. These stock solutions were used to prepare protein concentration series in PBS. These samples were stored at 4 °C until use. They were mixed with the QDs in a 1:1 volume ratio. The mixtures were kept for 10 min at room temperature before measurements were carried out in a 1 mm wide channel between two coverslips, formed by using 200 μm thick double-sided adhesive tape as spacer. From autocorrelation analysis of the recorded fluorescence emission time traces, the hydrodynamic radii, r_h, of the NPs were obtained as a function of protein concentration. The resulting binding curves were fitted with the model presented in section Quantitative Analysis of Protein Corona Formation on DHLA-QDs, eqs 2 and 3; the hydrodynamic radius of the bare NPs, $r_h(0)$, was treated as a global parameter for the measurements performed with HSA and HSAsuc because the QDs used were from the same batch. For the fit, the volume of HSA was taken to be the volume of an equilateral triangular prism with

sides of 8.4 nm and thickness 3.15 nm.[48] To test the reversibility of protein binding, proteins and QDs were mixed and diluted after the typical incubation time (10 min). After further equilibration for 90 min, FCS measurements were carried out as described above.

Cell Sample Preparations. HeLa cells were incubated with Dulbecco's modified Eagle's medium (DMEM, Invitrogen, Munich, Germany) with 10% fetal bovine serum and antibiotics (60 μg/mL penicillin, 100 μg/mL streptomycin) in an incubation chamber (Thermo Fischer Scientific, Hanau, Germany) at 37 °C, 5% CO_2. Cells were seeded on 8-well chamber slides (Nunc, Langenselbold, Germany) one day prior to the experiments, with ~15 000 cells per chamber. Before the kinetics experiment, cells were washed twice with PBS, and the membrane was stained for 5 min with 300 μL of 0.25 μg mL^{-1} CellMask DeepRed (Invitrogen, Munich, Germany). NPs were added after renewed washing (three times) with PBS and acquisition of images for background correction. For single images of the cells, cells were washed twice with PBS, and the nucleus was stained for 20 min with 300 μL of 0.25 μg mL^{-1} Hoechst (Hoechst 33342, Invitrogen). NPs were added after renewed washing (three times) with PBS and the cells were further incubated at 37 °C, 5% CO_2 for 2 h. Afterward, the cells were washed, the membrane was stained as described above and single images of the cells were recorded.

Live Cell Confocal Imaging. Cellular NP uptake was imaged with an Andor Revolution XD spinning disk confocal microscope (BFi OPTiLAS, Munich, Germany) as described.[84] For excitation, solid state lasers emitting at 532 nm (Sapphire 532LP, Coherent, Santa Clara, CA) and 640 nm (Cube 640-40C, Coherent) with 50 and 40 mW power, respectively, were used. QDs were illuminated for 100 ms with the 532 nm laser and a power of 60 μW, using a 607/36 nm detection filter. CellMask DeepRed was illuminated for 80 ms at 640 nm with a power of 60 μW and a 685/40 nm detection filter. For the quantitative analysis of QD uptake by HeLa cells, we acquired dual-color images of confocal cross sections at about half cell height.

Image Analysis. Custom-written software in MATLAB (The MathWorks, Natick, NY) was used to generate binary masks for both the membrane-associated regions as well as the intracellular space.[58,62] An adaptive Sobel filter was applied to the image of the stained membrane in the red channel to detect the cellular contour, which was further refined using gradient vector flow fields.[85] Finally, binary masks of the membrane-associated region and the intracellular space were applied to the nanoparticle image in the green channel to reveal the associated intensities.

To quantify the QD uptake kinetics, the fluorescence intensities in the two regions were determined as a function of time. To account for variations in cell size, the fluorescence was normalized with respect to the cross-sectional area of the cell. An average background fluorescence was determined outside the cells and subtracted. For each cell, the fluorescence intensities inside the cell and at the membrane were set to zero at $t = 0$, and the intensities at $t > 0$ were scaled by their maximal values, so that they represent relaxation curves ranging between 0 and 1. This treatment removes cell-to-cell variations of the uptake yield. Subsequently, the normalized kinetic traces were averaged over the entire ensemble of cells to determine the uptake rate. To enable a comparison of the absolute uptake of bare QDs and QDs coated with a protein corona, the kinetic traces were scaled by the average over all the maximum fluorescence intensity values observed, and a brightness scaling was applied as described in Supporting Information (Figure S3).

Conflict of Interest: The authors declare no competing financial interest.

Acknowledgment. This work was supported by the Deutsche Forschungsgemeinschaft (DFG) through the Center for Functional Nanostructures (CFN) and the Priority Program SPP1313. We thank Dr. Karin Nienhaus for valuable assistance.

Supporting Information Available: Full methodology and additional data (Figures S1–S3). This material is available free of charge via the Internet at http://pubs.acs.org.

REFERENCES AND NOTES

1. Treuel, L.; Jiang, X.; Nienhaus, G. U. New Views on Cellular Uptake and Trafficking of Manufactured Nanoparticles. *J. R. Soc. Interface* **2013**, *10*, 1742–5662.
2. Lunov, O.; Syrovets, T.; Röcker, C.; Tron, K.; Nienhaus, G. U.; Rasche, V.; Mailänder, V.; Landfester, K.; Simmet, T. Lysosomal Degradation of the Carboxydextran Shell of Coated Superparamagnetic Iron Oxide Nanoparticles and the Fate of Professional Phagocytes. *Biomaterials* **2010**, *31*, 9015–9022.
3. Asha Rani, P. V.; Low Kah Mun, G.; Hande, M. P.; Valiyaveettil, S. Cytotoxicity and Genotoxicity of Silver Nanoparticles in Human Cells. *ACS Nano* **2008**, *3*, 279–290.
4. de Paoli Lacerda, S. H.; Park, J. J.; Meuse, C.; Pristinski, D.; Becker, M. L.; Karim, A.; Douglas, J. F. Interaction of Gold Nanoparticles with Common Human Blood Proteins. *ACS Nano* **2010**, *4*, 365–379.
5. Cedervall, T.; Lynch, I.; Foy, M.; Berggård, T.; Donnelly, S. C.; Cagney, G.; Linse, S.; Dawson, K. A. Detailed Identification of Plasma Proteins Adsorbed on Copolymer Nanoparticles. *Angew. Chem., Int. Ed.* **2007**, *46*, 5754–5756.
6. Cedervall, T.; Lynch, I.; Lindman, S.; Berggård, T.; Thulin, E.; Nilsson, H.; Dawson, K. A.; Linse, S. Understanding the Nanoparticle-Protein Corona Using Methods to Quantify Exchange Rates and Affinities of Proteins for Nanoparticles. *Proc. Natl. Acad. Sci. U.S.A.* **2007**, *104*, 2050–2055.
7. Lundqvist, M.; Stigler, J.; Elia, G.; Lynch, I.; Cedervall, T.; Dawson, K. A. Nanoparticle Size and Surface Properties Determine the Protein Corona with Possible Implications for Biological Impacts. *Proc. Natl. Acad. Sci. U.S.A.* **2008**, *105*, 14265–14270.
8. Röcker, C.; Pötzl, M.; Zhang, F.; Parak, W. J.; Nienhaus, G. U. A Quantitative Fluorescence Study of Protein Monolayer Formation on Colloidal Nanoparticles. *Nat. Nanotechnol.* **2009**, *4*, 577–580.
9. Treuel, L.; Malissek, M.; Gebauer, J. S.; Zellner, R. The Influence of Surface Composition of Nanoparticles on Their Interactions with Serum Albumin. *ChemPhysChem* **2010**, *11*, 3093–3099.
10. Klein, J. Probing the Interactions of Proteins and Nanoparticles. *Proc. Natl. Acad. Sci. U.S.A.* **2007**, *104*, 2029–2030.
11. Leszczynski, J. Bionanoscience: Nano Meets Bio at the Interface. *Nat. Nanotechnol.* **2010**, *5*, 633–634.
12. Monopoli, M. P.; Walczyk, D.; Campbell, A.; Elia, G.; Lynch, I.; Baldelli Bombelli, F.; Dawson, K. A. Physical–Chemical Aspects of Protein Corona: Relevance to *in Vitro* and *in Vivo* Biological Impacts of Nanoparticles. *J. Am. Chem. Soc.* **2011**, *133*, 2525–2534.
13. Frauenfelder, H.; Nienhaus, G. U.; Johnson, J. B. Rate Processes in Proteins. *Ber. Bunsen-Ges. Phys. Chem.* **1991**, *95*, 272–278.
14. Aubin-Tam, M.-E.; Hamad-Schifferli, K. Gold Nanoparticle-Cytochrome c Complexes: The Effect of Nanoparticle Ligand Charge on Protein Structure. *Langmuir* **2005**, *21*, 12080–12084.
15. Roach, P.; Farrar, D.; Perry, C. C. Surface Tailoring for Controlled Protein Adsorption: Effect of Topography at the Nanometer Scale and Chemistry. *J. Am. Chem. Soc.* **2006**, *128*, 3939–3945.
16. Medintz, I. L.; Konnert, J. H.; Clapp, A. R.; Stanish, I.; Twing, M. E.; Mattoussi, H.; Mauro, J. M.; Deschamps, J. R. A Fluorescence Resonance Energy Transfer-Derived Structure of a Quantum Dot-Protein Bioconjugate Nanoassembly. *Proc. Natl. Acad. Sci. U.S.A.* **2004**, *101*, 9612–9617.
17. Vertegel, A. A.; Siegel, R. W.; Dordic, J. S. Silica Nanoparticle Size Influences the Structure and Enzymatic Activity of Adsorbed Lysozyme. *Langmuir* **2004**, *20*, 6800–6807.
18. Rodriguez, C. E.; Fukuto, J. M.; Taguchi, K.; Froines, J.; Cho, A. K. The Interactions of 9,10-Phenantrenequinone with Glyceraldehyde-3-phosphatedehydrogenase (GAPDH), a Potential Site for Toxic Actions. *Chem.–Biol. Interact.* **2005**, *155*, 97–110.
19. Lynch, I.; Dawson, K. A.; Linse, S. Detecting Cryptic Epitopes Created by Nanoparticles. *Science STKE* **2006**, *2006*, pe14.

20. Baron, M. H.; Revault, M.; Servagent-Noinville, S.; Abadie, J.; Qui-Quampoix, H. J. Chymotrypsin Adsorption on Montmorillonite: Enzymatic Activity and Kinetic FTIR Structural Analysis. *J. Colloid Interface Sci.* **1999**, *214*, 319–332.
21. Brandes, N.; Welzel, P. B.; Werner, C.; Kroh, L. W. Adsorption-Induced Conformational Changes of Proteins onto Ceramic Particles: Differential Scanning Calorimetry and FTIR Analysis. *J. Colloid Interface Sci.* **2006**, *299*, 56–69.
22. Nel, A. E.; Mädler, L.; Velegol, D.; Xia, T.; Hoek, E. M.; Somasundaran, P.; Klaessig, F.; Castranova, V.; Thompson, M. Understanding Biophysicochemical Interactions at the Nano-Bio Interface. *Nat. Mater.* **2009**, *8*, 543–557.
23. des Rieux, A.; Fievez, V.; Garinot, M.; Schneider, Y.-J.; Préat, V. Nanoparticles as Potential Oral Delivery Systems of Proteins and Vaccines: A Mechanistic Approach. *J. Controlled Release* **2006**, *116*, 1–27.
24. Yan, M.; Du, J.; Gu, Z.; Liang, M.; Hu, Y.; Zhang, W.; Priceman, S.; Wu, L.; Hong Zhou, Z.; Liu, H.; *et al.* A Novel Intracellular Protein Delivery Platform Based on Single-Protein Nanocapsules. *Nat. Nanotechnol.* **2009**, *5*, 48–53.
25. Liu, L.; Xu, K.; Wang, H.; Tan, P. K. J.; Fan, W.; Venkatraman, S. S.; Li, L.; Yang, Y.-Y. Self-Assembled Cationic Peptide Nanoparticles as an Efficient Antimicrobial Agent. *Nat. Nanotechnol.* **2009**, *4*, 457–463.
26. Nel, A.; Xia, T.; Mädler, L.; Li, N. Toxic Potential of Materials at the Nanolevel. *Science* **2006**, *311*, 622–627.
27. Kostarelos, K.; Bianco, A.; Prato, M. Promises, Facts and Challenges for Carbon Nanotubes in Imaging and Therapeutics. *Nat. Nanotechnol.* **2009**, *4*, 627–633.
28. Tasis, D.; Tagmatarchis, N.; Bianco, A.; Prato, M. Chemistry of Carbon Nanotubes. *Chem. Rev.* **2006**, *106*, 1105–1136.
29. Hamman, J. H.; Enslin, G. M.; Kotze, A. F. Oral Delivery of Peptide Drugs: Barriers and Developments. *BioDrugs* **2005**, *19*, 165–177.
30. Galindo-Rodriguez, S. A.; Allemann, E.; Fessi, H.; Doelker, E. Polymeric Nanoparticles for Oral Delivery of Drugs and Vaccines: A Critical Evaluation of *in Vivo* Studies. *Crit. Rev. Ther. Drug Carrier Syst.* **2005**, *22*, 419–464.
31. Ghosh, P.; Han, G.; De, M.; Kim, C. K.; Rotello, V. M. Gold Nanoparticles in Delivery Applications. *Adv. Drug Delivery Rev.* **2008**, *60*, 1307–1315.
32. Gan, Z. H.; Yu, D. H.; Zhong, Z. Y.; Liang, Q. Z.; Jing, X. B. Enzymatic Degradation of Poly(Epsilon-Caprolactone)/Poly(DL-Lactide) Blends in Phosphate Buffer Solution. *Polymer* **1999**, *40*, 2859–2862.
33. Leroueil-Le, V. M.; Fluckiger, L.; Kim, Y. I.; Hoffmann, M.; Maincent, P. Preparation and Characterisation of Nanoparticles Containing an Antihypertensive Agent. *Eur. J. Pharm. Biopharm.* **1998**, *46*, 137–143.
34. Balthasar, S.; Michaelis, K.; Dinauer, N.; von Kreuter, J.; Langer, K. Preparation and Characterisation of Antibody Modified Gelatin Nanoparticles as Drug Carrier System for Uptake in Lymphocytes. *Biomaterials* **2005**, *26*, 2723–2732.
35. Johnson, F. A.; Craig, D. Q.; Mercer, A. D. Characterization of the Block Structure and Molecular Weight of Sodium Alginates. *J. Pharm. Pharmacol.* **1997**, *49*, 639–643.
36. Fonseca, C.; Simoes, S.; Gaspar, R. Paclitaxel-Loaded PLGA Nanoparticles: Preperation, Physicochemical Charactertization and *in Vitro* Anti-Tumoral Activity. *J. Controlled Release* **2002**, *83*, 273–286.
37. Kumar Ravi, M. N.; Bakowsky, U.; Lehr, C. M. Preparation and Characterization of Cationic PLGA Nanospheres as DNA Carriers. *Biomaterials* **2004**, *25*, 1771–1777.
38. Dillen, K.; Vandervoort, J.; Van den Mooter, G.; Verheyden, L.; Ludwig, A. Factorial Design, Physicochemical Characterisation and Acitivity of Ciprofloxacin-PLGA Nanoparticles. *Int. J. Pharm.* **2004**, *275*, 171–187.
39. Govender, T.; Stolnik, S.; Garnett, M. C.; Illum, L.; Davis, S. S. PLGA Nanoparticles Prepared by Nanoprecipitation: Drug Loading and Release Studies of a Water Soluble Drug. *J. Controlled Release* **1999**, *57*, 171–185.
40. Lemoine, D.; Preat, V. Polymeric Nanoparticles as Delivery System for Influenza Virus Glycoproteins. *J. Controlled Release* **1998**, *54*, 15–27.
41. Langer, R. S.; Peppas, N. A. Present and Future Applications of Biomaterials in Controlled Drug Delivery Systems. *Biomaterials* **1981**, *2*, 201–214.
42. Miller, J. D.; Anderson, M. G. Therapeutic Effects of Leuprorelin Microspheres on Endometriosis and Uterine Leiomyomata. *Adv. Drug Delivery Rev.* **1997**, *60*, 179–155.
43. Ayalasomayajula, S. P.; Kompella, U. B. Subconjunctivally Administered Celecoxib-PLGA Microparticles Sustain Retinal Drug Levels and Alleviate Diabetes-Induced Oxidative Stress in a Rat Model. *Eur. J. Pharm. Biopharm.* **2005**, *511*, 191–198.
44. Kou, J. H.; Emmett, C.; Shen, P.; Aswani, S.; Iwamoto, T.; Vaghefi, F.; Cain, G.; Sanders, L. Bioerosion and Biocompatibility of Poly(*D,L*-Lactic-Co-Glycolic Acid). *J. Controlled Release* **1997**, *43*, 123–130.
45. Lee, S. Y.; Oh, J. H.; Kim, Y. H.; Kim, S. H.; Choi, J. W. *In Vivo* Conjunctival Reconstruction Using Modified PLGA Grafts for Decreased Scar Formation and Contraction. *Biomaterials* **2003**, *24*, 5049–5059.
46. Zhou, T.; Lewis, H.; Foster, R. E.; Schwendman, S. P. Development of a Multiple-Drug Delivery Implant for Intraocular Management of Proliferative Vitreoretinopathy. *J. Controlled Release* **1998**, *55*, 281–295.
47. Maffre, P.; Nienhaus, K.; Amin, F.; Parak, W. J.; Nienhaus, G. U. Characterization of Protein Adsorption onto Fept Nanoparticles Using Dual-Focus Fluorescence Correlation Spectroscopy. *Beilstein J. Nanotechnol.* **2011**, *2*, 374–383.
48. He, X. M.; Carter, D. C. Atomic Structure and Chemistry of Human Serum Albumin. *Nature* **1992**, *358*, 209–215.
49. Dolinsky, T. J.; Nielsen, J. E.; McCammon, J. A.; Baker, N. A. Pdb2pqr: An Automated Pipeline for the Setup of Poisson-Boltzmann Electrostatics Calculations. *Nucleic Acids Res.* **2004**, *32*, W665–W667.
50. Habeeb, A. F. S. Antigenicity of Chemically Modified Bovine Serum Albumin. *J. Immunol.* **1967**, *99*, 1264–1276.
51. Jansen, R. W.; Schols, D.; Pauwels, R.; Declercq, E.; Meijer, D. K. F. Novel, Negatively Charged, Human Serum Albumins Display Potent and Selective in-Vitro Anti-Human-Immunodeficiency-Virus Type-1 Activity. *Mol. Pharmacol.* **1993**, *44*, 1003–1007.
52. Hermanson, G. T. *Bioconjugate Techniques*; Academic Press: San Diego, CA, 1996; p 785.
53. Aitken, A.; Learmonth, M. Succinylation of Proteins. In *The Protein Protocols Handbook*; Walker, J., Ed.; Humana Press: Towota, NJ, 1996; pp 343−344.
54. Lamb, D. C.; Schenk, A.; Röcker, C.; Scalfi-Happ, C.; Nienhaus, G. U. Sensitivity Enhancement in Fluorescence Correlation Spectroscopy of Multiple Species Using Time-Gated Detection. *Biophys. J.* **2000**, *79*, 1129–1138.
55. Maiti, S.; Haupts, U.; Webb, W. W. Fluorescence Correlation Spectroscopy: Diagnostics for Sparse Molecules. *Proc. Natl. Acad. Sci. U.S.A.* **1997**, *94*, 11753–11757.
56. Zemanová, L.; Schenk, A.; Valler, M. J.; Nienhaus, G. U.; Heilker, R. Confocal Optics Microscopy for Biochemical and Cellular High-Throughput Screening. *Drug Discovery Today* **2003**, *8*, 1085–1093.
57. Treuel, L.; Nienhaus, G. U. Toward a Molecular Understanding of Nanoparticle−Protein Interactions. *Biophys. Rev.* **2012**, *4*, 137–147.
58. Jiang, X.; Röcker, C.; Hafner, M.; Brandholt, S.; Dörlich, R. M.; Nienhaus, G. U. Endo- and Exocytosis of Zwitterionic Quantum Dot Nanoparticles by Live HeLa Cells. *ACS Nano* **2010**, *4*, 6787–6797.
59. Jiang, X.; Dausend, J.; Hafner, M.; Musyanovych, A.; Röcker, C.; Landfester, K.; Mailänder, V.; Nienhaus, G. U. Specific Effects of Surface Amines on Polystyrene Nanoparticles in Their Interactions with Mesenchymal Stem Cells. *Biomacromolecules* **2010**, *11*, 748–753.
60. Jiang, X.; Musyanovych, A.; Röcker, C.; Landfester, K.; Mailänder, V.; Nienhaus, G. U. Specific Effects of Surface Carboxyl Groups on Anionic Polystyrene Particles in Their Interactions with Mesenchymal Stem Cells. *Nanoscale* **2011**, *3*, 2028–2035.
61. Wang, T.; Bai, J.; Jiang, X.; Nienhaus, G. U. Cellular Uptake of Nanoparticles by Membrane Penetration: A Study

Combining Confocal Microscopy with FTIR Spectroelectrochemistry. *ACS Nano* **2012**, *6*, 1251–1259.
62. Jiang, X.; Weise, S.; Hafner, M.; Röcker, C.; Zhang, F.; Parak, W. J.; Nienhaus, G. U. Quantitative Analysis of the Protein Corona on Fept Nanoparticles Formed by Transferrin Binding. *J. R. Soc. Interface* **2010**, *7*, S5–S13.
63. Salvati, A.; Pitek, A. S.; Monopoli, M. P.; Prapainop, K.; Bombelli, F. B.; Hristov, D. R.; Kelly, P. M.; Aberg, C.; Mahon, E.; Dawson, K. A. Transferrin-Functionalized Nanoparticles Lose Their Targeting Capabilities When a Biomolecule Corona Adsorbs on the Surface. *Nat, Nanotechnol.* **2013**, *8*, 137–143.
64. Lesniak, A.; Salvati, A.; Santos-Martinez, M. J.; Radomski, M. W.; Dawson, K. A.; Åberg, C. Nanoparticle Adhesion to the Cell Membrane and Its Effect on Nanoparticle Uptake Efficiency. *J. Am. Chem. Soc.* **2013**, *135*, 1438–1444.
65. Lesniak, A.; Fenaroli, F.; Monopoli, M. P.; Åberg, C.; Dawson, K. A.; Salvati, A. Effects of the Presence or Absence of a Protein Corona on Silica Nanoparticle Uptake and Impact on Cells. *ACS Nano* **2012**, *6*, 5845–5857.
66. Shang, L.; Dörlich, R. M.; Trouillet, V.; Bruns, M.; Nienhaus, G. U. Ultrasmall Fluorescent Silver Nanoclusters: Protein Adsorption and Its Effects on Cellular Responses. *Nano Res.* **2012**, *5*, 531–542.
67. Lunov, O.; Syrovets, T.; Loos, C.; Beil, J.; Delacher, M.; Tron, K.; Nienhaus, G. U.; Musyanovych, A.; Mailänder, V.; Landfester, K.; Simmet, T. Differential Uptake of Functionalized Polystyrene Nanoparticles by Human Macrophages and a Monocytic Cell Line. *ACS Nano* **2011**, *5*, 1657–1669.
68. Patel, P. C.; Giljohann, D. A.; Daniel, W. L.; Zheng, D.; Prigodich, A. E.; Mirkin, C. A. Scavenger Receptors Mediate Cellular Uptake of Polyvalent Oligonucleotide-Functionalized Gold Nanoparticles. *Bioconjugate Chem.* **2010**, *21*, 2250–2256.
69. Lunov, O.; Zablotskii, V.; Syrovets, T.; Röcker, C.; Tron, K.; Nienhaus, G. U.; Simmet, T. Modeling Receptor-Mediated Endocytosis of Polymer-Functionalized Iron Oxide Nanoparticles by Human Macrophages. *Biomaterials* **2011**, *32*, 547–555.
70. Yang, L.; Shang, L.; Nienhaus, G. U. Mechanistic Aspects of Fluorescent Gold Nanocluster Internalization by Live HeLa Cells. *Nanoscale* **2013**, *5*, 1537–1543.
71. Roser, M.; Fischer, D.; Kissel, T. Surface-Modified Biodegradable Albumin Nano- and Microspheres. II: Effect of Surface Charges on *in Vitro* Phagocytosis and Biodistribution in Rats. *Eur. J. Pharm. Biopharm.* **1998**, *46*, 255–263.
72. Aggarwal, P.; Hall, J. B.; McLeland, C. B.; Dobrovolskaia, M. A.; McNeil, S. E. Nanoparticle Interaction with Plasma Proteins as It Relates to Particle Biodistribution, Biocompatibility and Therapeutic Efficacy. *Adv. Drug Delivery Rev.* **2009**, *61*, 428–437.
73. Owens, D. E., III; Peppas, N. A. Opsonization, Biodistribution, and Pharmacokinetics of Polymeric Nanoparticles. *Int. J. Pharm.* **2006**, *307*, 93–102.
74. Tenzer, S.; Docter, D.; Rosfa, S.; Wlodarski, A.; Kuharev, J.; Rekik, A.; Knauer, S. K.; Bantz, C.; Nawroth, T.; Bier, C.; *et al.* Nanoparticle Size Is a Critical Physicochemical Determinant of the Human Blood Plasma Corona: A Comprehensive Quantitative Proteomic Analysis. *ACS Nano* **2011**, *5*, 7155–7167.
75. Brancolini, G.; Kokh, D. B.; Calzolai, L.; Wade, R. C.; Corni, S. Docking of Ubiquitin to Gold Nanoparticles. *ACS Nano* **2012**, *6*, 9863–9878.
76. Gebauer, J. S.; Malissek, M.; Simon, S.; Knauer, S. K.; Maskos, M.; Stauber, R. H.; Peukert, W.; Treuel, L. Impact of the Nanoparticle-Protein Corona on Colloidal Stability and Protein Structure. *Langmuir* **2012**, *28*, 9673–9679.
77. Treuel, L.; Malissek, M.; Grass, S.; Diendorf, J.; Mahl, D.; Meyer-Zaika, W.; Epple, M. Quantifying the Influence of Polymer Coatings on the Serum Albumin Corona Formation around Silver and Gold Nanoparticles. *J. Nanopart. Res.* **2012**, *14*, 1–12.
78. Breus, V. V.; Heyes, C. D.; Tron, K.; Nienhaus, G. U. Zwitterionic Biocompatible Quantum Dots for Wide pH Stability and Weak Nonspecific Binding to Cells. *ACS Nano* **2009**, *3*, 2573–2580.
79. Clapp, A. R.; Goldman, E. R.; Mattoussi, H. Capping of CdSe-ZnS Quantum Dots with Dhla and Subsequent Conjugation with Proteins. *Nat. Protocols* **2006**, *1*, 1258–1266.
80. Shang, L.; Yang, L.; Seiter, J.; Heinle, M.; Brenner-Weiss, G.; Gerthsen, D.; Nienhaus, G. U. Nanoparticles Interacting with Proteins and Cells: A Systematic Study of Protein Surface Charge Effects. *Adv. Mater. Interfaces* **2013**, 10.1002/admi.201300079.
81. Heyes, C. D.; Kobitski, A. Y.; Amirgoulova, E. V.; Nienhaus, G. U. Biocompatible Surfaces for Specific Tethering of Individual Protein Molecules. *J. Phys. Chem. B* **2004**, *108*, 13387–13394.
82. Kobitski, A. Y.; Hengesbach, M.; Helm, M.; Nienhaus, G. U. Sculpting an RNA Conformational Energy Landscape by a Methyl Group Modification—a Single-Molecule FRET Study. *Angew. Chem., Int. Ed.* **2008**, *47*, 4326–4330.
83. Müller, C. B.; Loman, A.; Pacheco, V.; Koberling, F.; Willbold, D.; Richtering, W.; Enderlein, J. Precise Measurement of Diffusion by Multi-Color Dual-Focus Fluorescence Correlation Spectroscopy. *Europhys. Lett.* **2008**, *83*, 46001.
84. Shang, L.; Yang, L.; Stockmar, F.; Popescu, R.; Trouillet, V.; Bruns, M.; Gerthsen, D.; Nienhaus, G. U. Microwave-Assisted Rapid Synthesis of Luminescent Gold Nanoclusters for Sensing Hg^{2+} in Living Cells Using Fluorescence Imaging. *Nanoscale* **2012**, *4*, 4155–4160.
85. Chenyang, X.; Prince, J. L. Snakes, Shapes, and Gradient Vector Flow. *IEEE Trans. Image Process.* **1998**, *7*, 359–369.